Euro. Jnl of Applied Mathematics (2004), *vol.* 15, *pp.* 609–623. © 2004 Cambridge University Press
doi:10.1017/S0956792504005790 Printed in the United Kingdom

Antisymmetric capillary waves in electrified fluid sheets

D. T. PAPAGEORGIOU[1] and J.-M. VANDEN-BROECK[2]

[1] *Department of Mathematical Sciences and Center for Applied Mathematics and Statistics, New Jersey Institute of Technology, University Heights, Newark, NJ 07102, USA*
email: depapa@oak.njit.edu
[2] *School of Mathematics, University of East Anglia, Norwich NR4 7TJ, UK*

(*Received 8 January 2004; revised 24 May 2004*)

Capillary waves on fluid sheets are computed in the presence of a uniform electric field acting horizontally with respect to the undisturbed configuration. The fluid is taken to be inviscid, incompressible and nonconducting. In previous work (Papageorgiou & Vanden-Broeck [14]) symmetric travelling waves were investigated. In this paper we show that there are in addition antisymmetric waves. These waves are calculated numerically for arbitrary amplitudes and wavelengths and the effect of the electric field is studied. The numerical procedure is based on a reformulation of the problem as a system of nonlinear integro–differential equations.

1 Introduction

Free liquid films arise in different physical and technological applications in chemical and biomedical engineering, for example. The nonlinear phenomena associated with large interfacial deflections and possible rupture, are of interest in the fundamental understanding of such flows. Physical applications have been discussed by Maldarelli *et al.* ([12], Ruckenstein & Jain [15] and Scheludko [17], among others.

The linear stability of inviscid free liquid sheets to two-dimensional disturbances was considered by Taylor [19] who derived dispersion relations for both symmetric (varicose) and antisymmetric (sinuous) modes. Viscosity was included by Maldarelli *et al.* [12] and Ruckenstein & Jain [15], and is found to damp the dispersive waves. In all these studies gravity is absent and surface tension is present. In the case of a free surface above an infinitely deep inviscid liquid, exact nonlinear traveling capillary waves were found by Crapper [5]. These solutions were extended to layers of finite thickness by Kinnersley [11], who constructed nonlinear symmetric waves (for inviscid flows these also describe waves over a horizontal solid surface), as well as nonlinear antisymmetric waves. Additional exact solutions were recently found by Crowdy [6] for waves on a fluid annulus. Further solutions were obtained numerically by Blyth & Vanden-Broeck [1, 2]. For the related problem including gravity, gravity-capillary waves in irrotational fluids have been computed numerically by (among others) Schwartz & Vanden-Broeck [18], Chen & Saffman [4], Hogan [7] and Hunter & Vanden-Broeck [8]; calculations when vorticity is present are reported in Kang & Vanden-Broeck [10].

https://doi.org/10.1017/S0956792504005790 Published online by Cambridge University Press

The presence of horizontal electric fields acting on fluid layers has been considered by Tilley *et al.* [20] and Savettaseranee *et al.* [16] who derive and study nonlinear long wave models describing inviscid and viscous flows respectively. The long-wave approximation was dropped by Papageorgiou & Vanden-Broeck [14], who use boundary integral methods to construct nonlinear symmetric traveling waves. These authors also present an alternative derivation of long-wave models and compare their solutions with the numerically constructed ones. Agreement is found to be excellent and the results establish the importance of traveling wave solutions of the model one-dimensional equations.

The calculation of antisymmetric solutions of the full problem when an electric field acts, has not been studied. In the present work we make no approximations on the competing length scales and address the problem of capillary waves driven by an electric field parallel to the fluid layer. The internal and external electric fields are fully accounted for, as is the incompressible irrotational fluid motion inside the layer. We use boundary integral methods to construct antisymmetric traveling waves of arbitrary amplitudes and periods and study the effects of the physical parameters on these waves.

The article is organized as follows: § 2 describes the governing equations and gives the exact dimensionless problem. § 3 reformulates the problem in terms of integral equations and § 4 describes our numerical methods. § 5 presents numerical solutions for a range of physical parameters and § 6 is devoted to concluding remarks.

2 Governing equations

We consider a liquid layer of undisturbed thickness $2d$ which is bounded by free surfaces at $y = S(x,t)$ and $y = \bar{S}(x,t)$ (see Figure 1). We include the effect of the surface tension σ at the interfaces but we neglect gravity (the latter assumption holds if the Bond number, $(\rho g d^2)/\sigma \ll 1$). We also assume that a applied uniform electric field given by $\mathbf{E}_0 = -(V_0/2L)\mathbf{i}$, is acting, where V_o is the characteristic voltage drop over a characteristic distance L. We introduce the dimensional fluid and voltage potentials ϕ and $V^{(1,2)}$, respectively. These potentials satisfy Laplace's equation

$$\nabla^2\phi(x,y;t) = 0, \tag{2.1}$$

$$\nabla^2 V^{(1,2)}(x,y;t) = 0, \tag{2.2}$$

where in what follows superscripts 1, 2 denote the regions bounded by and outside of the moving interfaces (see Figure 1). The electric fields are $\mathbf{E}^{(1,2)} = -\nabla V^{(1,2)}$. As $|y| \to \infty$, $\frac{\partial V^{(2)}}{\partial x} \to V_o/(2L)$.

In previous work, we considered symmetric solutions about the centerline $y = 0$. This yields $\bar{S}(x,t) = -S(x,t)$. In this paper we construct antisymmetric solutions for which

$$\bar{S}(x,t) = -S\left(\frac{\lambda}{2} + x, t\right) \tag{2.3}$$

$$\phi(x,\bar{S},t) = \phi\left(\frac{\lambda}{2} + x, S, t\right) \tag{2.4}$$

$$V^{(1,2)}(x,\bar{S},t) = V^{(1,2)}\left(\frac{\lambda}{2} + x, S, t\right) \tag{2.5}$$

https://doi.org/10.1017/S0956792504005790 Published online by Cambridge University Press

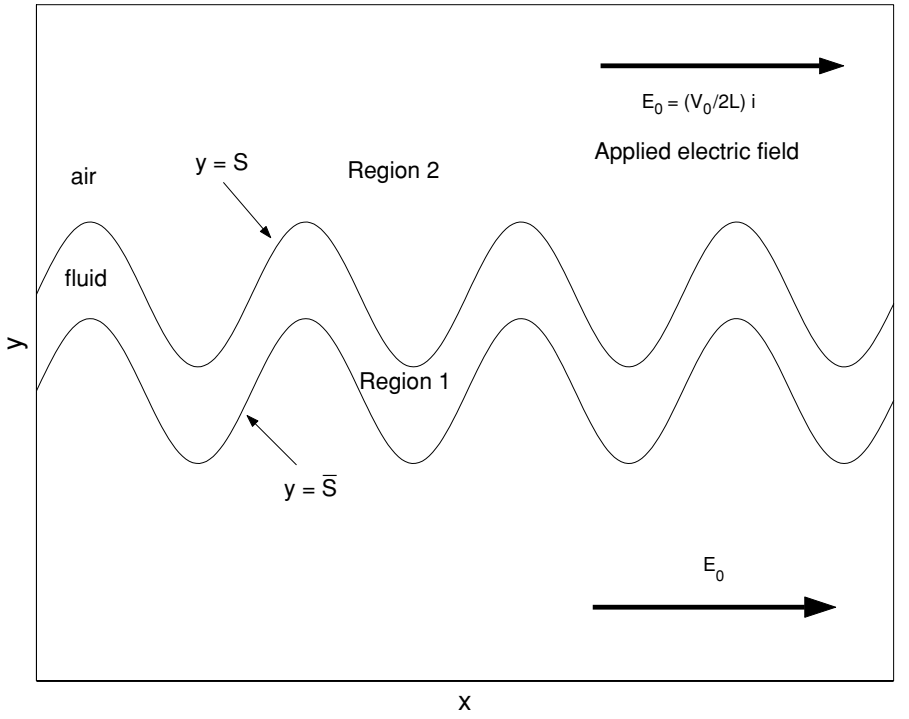


FIGURE 1. Schematic of the problem. The undisturbed layer has thickness $2d$ and region 2 extends to infinity.

Here λ is the wavelength of the wave. Relation (2.3) shows that the lower profile of the wave is obtained by reflecting $y = S(x,t)$ into the line $y = 0$ and shifting it by $\lambda/2$.

The boundary conditions at the free surfaces $y = S$ and $y = \bar{S}$ are the kinematic condition, continuity of normal stresses, and the continuity of the normal component of the displacement field ($\epsilon\mathbf{E}$) and tangential components of the electric field (we note that for nonconducting inviscid fluids the tangential stress balance is satisfied automatically). These are at $y = S(x,t)$:

$$S_t + \phi_x S_x - \phi_y = 0 \tag{2.6}$$

$$[\mathbf{n}\cdot\mathbf{T}\cdot\mathbf{n}]_2^1 = \sigma \mathrm{div}\mathbf{n} \tag{2.7}$$

$$[\epsilon\mathbf{E}\cdot\mathbf{n}]_2^1 = 0 \tag{2.8}$$

$$[\mathbf{E}\cdot\mathbf{t}]_2^1 = 0, \tag{2.9}$$

where $[\cdot]_2^1$ denotes the jump in the quantity as the interface is crossed from the fluid region, the vectors $\mathbf{n}$, $\mathbf{t}$ are the outward pointing normal and tangent to the interface respectively, and the stress tensor $\mathbf{T}$ is given by

$$T_{ij} = -p\delta_{ij} + \mathscr{E}_{ij},$$
$$\mathscr{E}_{ij} = \epsilon\left(E_iE_j - \frac{1}{2}|\mathbf{E}|^2\delta_{ij}\right). \tag{2.10}$$

https://doi.org/10.1017/S0956792504005790 Published online by Cambridge University Press

The first term in (2.10) is the inviscid hydrodynamic contribution and the second term arises from interfacial electric field stresses given by the Maxwell stress tensor (see Jackson [9, Chap. 6]). The parameters ϵ_1, ϵ_2 are the dielectric constants in regions 1 and 2 respectively. The same boundary conditions (with $S(x,t)$ replaced by $\bar{S}(x,t)$) hold at $y = \bar{S}(x,t)$. We do not write the boundary conditions at $y = \bar{S}(x,t)$ because they will not be used explicitly in the numerical procedure.

The Euler equations can be integrated to yield a Bernoulli equation at the interface. The pressure in region 2 is ambient and equal to a constant and on elimination of the pressure jump across the interface from (2.7), we arrive at the following Bernoulli boundary condition:

$$\rho_1\left(\phi_t + \frac{1}{2}|\nabla\phi|^2\right) + \frac{1}{1+S_x^2}\left\{S_x^2\,[\mathscr{E}_{11}]_2^1 - 2S_x\,[\mathscr{E}_{12}]_2^1 + [\mathscr{E}_{22}]_2^1\right\} = \frac{\sigma S_{xx}}{\left(1+S_x^2\right)^{3/2}} + K_p. \quad (2.11)$$

The Maxwell stresses appearing in (2.11) are given by

$$\mathscr{E}_{11} = \frac{\epsilon}{2}\left(V_x^2 - V_y^2\right), \qquad \mathscr{E}_{12} = \epsilon V_x V_y, \qquad \mathscr{E}_{22} = \frac{\epsilon}{2}\left(V_y^2 - V_x^2\right), \quad (2.12)$$

and superscripts 1 and 2 are implied where appropriate in (2.12). For the undisturbed state ($\phi = 0$, $S = d$), the constant $K_p = \frac{V_0^2}{8}(\epsilon_2 - \epsilon_1)$. This constant is related to the polarization pressure induced on fluid interfaces by the electric field (see Melcher & Schwarz [13]), and can be eliminated by differentiation of (2.11) with respect to x, for example. In what follows we denote the ratio of inside to outside permittivities by $\epsilon_p = \frac{\epsilon_1}{\epsilon_2}$.

2.1 Dimensionless equations

The equations and boundary conditions are made dimensionless using an outer length scale L to measure distances:

$$x = Lx', \quad y = Ly', \quad S = LS', \quad t = \sqrt{\frac{\rho_1 L^3}{\sigma}}t', \quad \phi = \sqrt{\frac{\sigma L}{\rho_1}}\phi', \quad V = V_0 V'. \quad (2.13)$$

We substitute (2.13) into the governing equations (2.1)–(2.2) and interfacial conditions (2.6)–(2.9), and drop the primes. With this choice of reference scales the undisturbed interface is located at $y = \frac{d}{L} = \delta$. In the numerical construction of traveling waves of arbitrary amplitude, we fix $\delta = 1$, that is the wave amplitude and wavelength are comparable. The fluid and voltage potentials satisfy the Laplace equations

$$\phi_{xx} + \phi_{yy} = 0, \quad (2.14)$$

$$V_{xx}^{(1,2)} + V_{yy}^{(1,2)} = 0. \quad (2.15)$$

The kinematic, Bernoulli and continuity of the normal displacement field and tangential electric field boundary conditions, evaluated at $y = S(x,t)$ become

$$S_t + \phi_x S_x - \phi_y = 0, \quad (2.16)$$

$$\phi_t + \frac{1}{2}\left(\phi_x^2 + \phi_y^2\right) + \frac{E_b}{1+S_x^2}\left\{\frac{1}{2}S_x^2[\mathscr{M}_{11}]_2^1 - 2S_x[\mathscr{M}_{12}]_2^1 + \frac{1}{2}[\mathscr{M}_{22}]_2^1\right\} = \frac{S_{xx}}{\left(1+S_x^2\right)^{3/2}} + \bar{K}_p. \quad (2.17)$$

https://doi.org/10.1017/S0956792504005790 Published online by Cambridge University Press

$$\epsilon_p\left(V_y^{(1)} - S_x V_x^{(1)}\right) = V_y^{(2)} - S_x V_x^{(2)} \tag{2.18}$$

$$V_x^{(1)} + S_x V_y^{(1)} = V_x^{(2)} + S_x V_y^{(2)}, \tag{2.19}$$

where the parameter $E_b = (\epsilon_2 V_o^2)/(\sigma L)$ is the ratio of the electrically induced pressure compared to capillary forces; we call this an electric capillary number. For the undisturbed state, $\bar{K}_p = \frac{E_b}{8}(1-\epsilon_p)$. The stress components in (2.17) are given by

$$\mathscr{M}_{11}^{(1,2)} = \left\{\frac{\epsilon}{\epsilon_2}\left[V_x^2 - V_y^2\right]\right\}^{(1,2)}, \tag{2.20}$$

$$\mathscr{M}_{12}^{(1,2)} = \left\{\frac{\epsilon}{\epsilon_2} V_x V_y\right\}^{(1,2)}, \tag{2.21}$$

$$\mathscr{M}_{22}^{(1,2)} = \left\{\frac{\epsilon}{\epsilon_2}\left[-V_x^2 + V_y^2\right]\right\}^{(1,2)}. \tag{2.22}$$

2.2 Linear theory

An exact trivial solution of the dimensionless problem is $S = \delta$, $\bar{S} = -\delta$, $\mathbf{u} = 0$ and $V^{(1,2)} = x/2$. We linearize the system (2.14)–(2.19). The antisymmetry conditions (2.3)–(2.5) give

$$\phi(x, -\delta, t) = \phi\left(\frac{\lambda}{2} + x, \delta, t\right), \tag{2.23}$$

$$V^{1,2}(x, -\delta, t) = V^{1,2}\left(\frac{\lambda}{2} + x, \delta, t\right). \tag{2.24}$$

We choose the origin $x = 0$ so that the equation of the free surface profile can be written as

$$S(x,t) = \delta + \delta' D\cos(kx - \omega t), \tag{2.25}$$

where D is a constant, δ' is the linearisation parameter, $k = 2\pi/\lambda$ is the wavenumber and ω the frequency. Since $k\lambda/2 = \pi$, the antisymmetry condition (2.3) is satisfied. Solving (2.14) by separation of variables and using the linearised kinematic boundary condition $\eta_t = \phi_y$ on $y = \delta$ yields

$$\phi(x,y,t) = \delta'[C\sinh(ky) + E\cosh(ky)]\sin(kx - \omega t) \tag{2.26}$$

where C and E are constants. Relation (2.23) is satisfied by choosing $E = 0$. Similarly we find by solution of (2.15) that

$$V^{(1)}(x,y,t) = \delta' A\sinh(ky)\sin(kx - \omega t), \tag{2.27}$$

$$V^{(2)}(x,y,t) = \delta' B\exp(-|ky|)\sin(kx - \omega t)\mathrm{sgn(y)}, \tag{2.28}$$

where A and B are constants. Using these solutions into the linearized kinematic, Bernoulli and electric field boundary conditions at the undisturbed level $S = \delta$, gives four

https://doi.org/10.1017/S0956792504005790 Published online by Cambridge University Press

homogeneous equations for the constants A, B, C, D. This leads to the eigenrelation

$$\omega^2 = \frac{E_b(1-\epsilon_p)^2}{4}\frac{k^3\coth k\delta}{\epsilon_p k\coth k\delta + |k|} + k^3\coth k\delta. \tag{2.29}$$

In the absence of an electric field, $E_b = 0$, we recover the linear dispersion relation for capillary waves on a fluid layer (Taylor [19]).

3 Reformulation as integral equations

We consider a train of waves of wavelength λ travelling at a constant velocity c in a two-fluid system. Precise definitions of c and of the thickness will be given later. We choose a frame of reference in which the flow is steady and we introduce cartesian coordinates with the x-axis parallel to the centreline of the undisturbed uniform layer and the origin at the centerline. We describe the free surface parametrically by $x = X(s)$ and $y = Y(s)$ where s is the arclength. Therefore

$$X'^2(s) + Y'^2(s) = 1 \tag{3.1}$$

We choose $x = s = 0$ at a crest and we express $X(s)$ and $Y(s)$ in terms of $X'(s)$ and $Y'(s)$ as

$$X(s) = \int_0^s X'(r)\,dr \tag{3.2}$$

$$Y(s) = \alpha + \int_0^s Y'(r)\,dr \tag{3.3}$$

Here α is the ordinate of the crests.

Next we rewrite (2.17) in the new frame of reference as

$$\frac{1}{2}(\phi_x^2 + \phi_y^2) + \frac{E_b}{1+S_x^2}\left\{\frac{1}{2}S_x^2[\mathscr{M}_{11}]_2^1 - 2S_x[\mathscr{M}_{12}]_2^1 + \frac{1}{2}[\mathscr{M}_{22}]_2^1\right\}$$
$$= Y''(s)X'(s) - X''(s)Y'(s) + B \tag{3.4}$$

where B is a constant to be found as part of the solution.

The horizontal and vertical components, u and v of the velocity in the fluid 1 are given by

$$u = \frac{\partial\phi}{\partial x}, \tag{3.5}$$

$$v = \frac{\partial\phi}{\partial y}. \tag{3.6}$$

We define the depth as the ordinate of the mean level of the interface. Therefore, we impose

$$\int_0^b Y(s)X'(s)\,ds = \delta. \tag{3.7}$$

Here b is the length of the interface in one wavelength.

We also define the velocity c by the formula (see Papageorgiou & Vanden-Broeck [14])

$$c = \frac{1}{\lambda}\int_0^b (uX'(s) + vY'(s))\,ds. \tag{3.8}$$

https://doi.org/10.1017/S0956792504005790 Published online by Cambridge University Press

As $y \to \infty$, $V_x^{(2)}$ approaches $1/2$. Since $V^{(2)}$ satisfies Laplace's equation, we have

$$\int_0^b \left(V_x^{(2)} X'(s) + V_y^{(2)} Y'(s)\right) ds = \int_0^\lambda V_x^{(2)}\, dx \tag{3.9}$$

where the integral on the right hand side is taken at a level y constant. Taking the limit as this constant approaches infinity we obtain

$$\frac{1}{2} = \frac{1}{\lambda} \int_0^b \left(V_x^{(2)} X'(s) + V_y^{(2)} Y'(s)\right) ds \tag{3.10}$$

To solve the problem we need to address the three Laplace equations (2.14)–(2.15) subject to the nonlinear boundary conditions (2.16)–(2.19). An efficient way to handle this problem is to cast the three Laplace equations into integral equations on the interface. These equations together with the boundary conditions are solved numerically as described in § 4. The obvious advantage of this formulation is that mesh points are required only on the interface. Further more, using periodicity and symmetry of solutions, enables us to discretize only half a wavelength.

We map the fluid in region 1 within $-\lambda/2 < x < \lambda/2$ from the $z = x + iy$-plane into the interior of an annular region of the ζ-plane by the transformation

$$\zeta = e^{-\frac{2i\pi z}{\lambda}}. \tag{3.11}$$

We seek the complex velocity $W = u - iv$ as an analytic function of ζ. Since W is periodic in x with period λ, it gives rise to a single valued analytic function of ζ. The boundaries of the annular region consist of the upper and lower free interfaces. We apply Cauchy's integral equation formula to the function $W = u - iv$ in the annular region of the ζ-plane. This yields

$$W(\zeta) = -\frac{1}{\pi i} \oint_{C_o} \frac{W(\mu)}{\mu - \zeta}\, d\mu, \tag{3.12}$$

where ζ is on the free surface and C_o denotes the boundaries of the annular region. The integral in (3.12) is a Cauchy-principal value.

Let $\beta = \frac{2\pi}{\lambda}$, $V_1 = u(s)X'(s) + v(s)Y'(s)$, $V_2 = u(s)Y'(s) - v(s)X'(s)$, $\tilde{V}_1 = u(\frac{b}{2} - s)X'(\frac{b}{2} - s) + v(\frac{b}{2} - s)Y'(\frac{b}{2} - s)$, $\tilde{V}_2 = u(\frac{b}{2} - s)Y'(\frac{b}{2} - s) - v(\frac{b}{2} - s)X'(\frac{b}{2} - s)$, $Y_\pm = Y(r) \pm Y(s)$, $X_\pm = X(r) \pm X(s)$, $\tilde{Y}_\pm = Y(r) \pm Y(\frac{b}{2} - s)$ and $\tilde{X}_\pm = X(r) \pm [\frac{\lambda}{2} - X(\frac{b}{2} - s)]$. Then taking the real part of (3.12) yields after some algebra

$$\begin{aligned}
\frac{\lambda}{2} u(r) = &\int_0^{\frac{b}{2}} \frac{V_1(1 - e^{\beta Y_-}\cos(\beta X_+)) - V_2(e^{\beta Y_-}\sin(\beta X_+))}{1 + e^{2\beta Y_-} - 2e^{\beta Y_-}\cos(\beta X_+)}\, \mathrm{ds} \\
&+ \int_0^{\frac{b}{2}} \frac{V_1(1 - e^{\beta Y_-}\cos(\beta X_-)) + V_2(e^{\beta Y_-}\sin(\beta X_-))}{1 + e^{2\beta Y_-} - 2e^{\beta Y_-}\cos(\beta X_-)}\, \mathrm{ds} \\
&- \int_0^{\frac{b}{2}} \frac{\tilde{V}_1(1 - e^{\beta \tilde{Y}_+}\cos(\beta \tilde{X}_-)) - \tilde{V}_2(e^{\beta \tilde{Y}_+}\sin(\beta \tilde{X}_-))}{1 + e^{2\beta \tilde{Y}_+} - 2e^{\beta \tilde{Y}_+}\cos(\beta \tilde{X}_-)}\, \mathrm{ds} \\
&- \int_0^{\frac{b}{2}} \frac{\tilde{V}_1(1 - e^{\beta \tilde{Y}_+}\cos(\beta \tilde{X}_+)) + \tilde{V}_2(e^{\beta \tilde{Y}_+}\sin(\beta \tilde{X}_+))}{1 + e^{2\beta \tilde{Y}_+} - 2e^{\beta \tilde{Y}_+}\cos(\beta \tilde{X}_+)}\, \mathrm{ds}.
\end{aligned} \tag{3.13}$$

https://doi.org/10.1017/S0956792504005790 Published online by Cambridge University Press

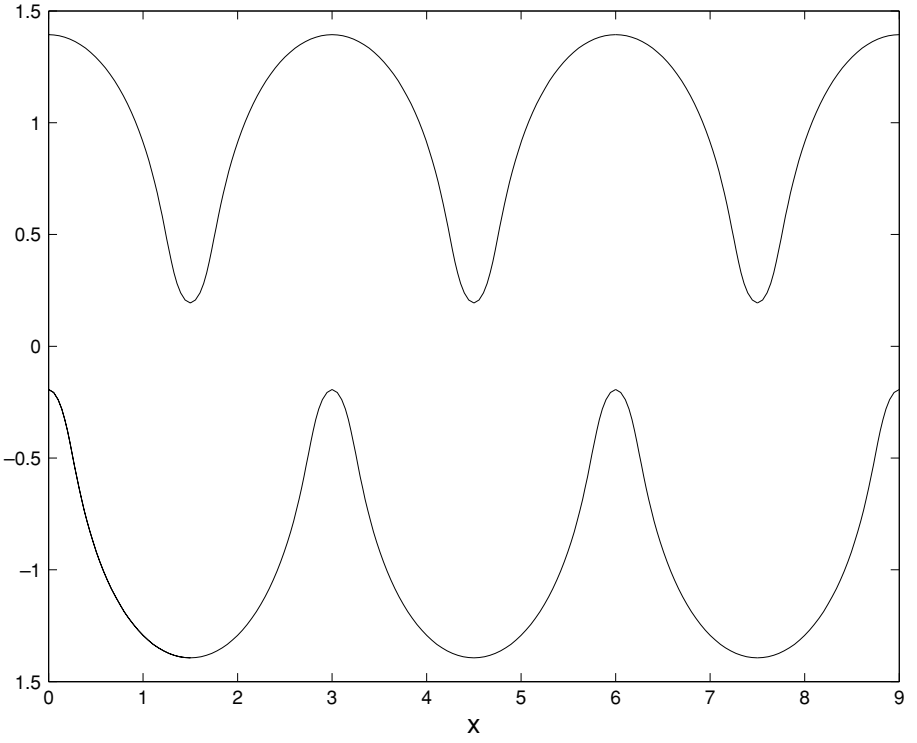


FIGURE 2. A typical antisymmetric traveling wave for $\lambda = 3$, $E_b = 3$, $h = 0.5$ and $\epsilon_p = 0.5$.

Similarly we derive

$$\frac{\lambda}{2}V_x^{(1)}(r) = \int_0^{\frac{b}{2}} \frac{A_1(1 - e^{\beta Y_-}\cos(\beta X_+)) - A_2(e^{\beta Y_-}\sin(\beta X_+))}{1 + e^{2\beta Y_-} - 2e^{\beta Y_-}\cos(\beta X_+)}\,\mathrm{ds}$$
$$+ \int_0^{\frac{b}{2}} \frac{A_1(1 - e^{\beta Y_-}\cos(\beta X_-)) + A_2(e^{\beta Y_-}\sin(\beta X_-))}{1 + e^{2\beta Y_-} - 2e^{\beta Y_-}\cos(\beta X_-)}\,\mathrm{ds}$$
$$- \int_0^{\frac{b}{2}} \frac{\tilde{A}_1(1 - e^{\beta \tilde{Y}_+}\cos(\beta \tilde{X}_-)) - \tilde{A}_2(e^{\beta \tilde{Y}_+}\sin(\beta \tilde{X}_-))}{1 + e^{2\beta \tilde{Y}_+} - 2e^{\beta \tilde{Y}_+}\cos(\beta \tilde{X}_-)}\,\mathrm{ds}$$
$$- \int_0^{\frac{b}{2}} \frac{\tilde{A}_1(1 - e^{\beta \tilde{Y}_+}\cos(\beta \tilde{X}_+)) + A_2(e^{\beta \tilde{Y}_+}\sin(\beta \tilde{X}_+))}{1 + e^{2\beta \tilde{Y}_+} - 2e^{\beta \tilde{Y}_+}\cos(\beta \tilde{X}_+)}\,\mathrm{ds}. \qquad (3.14)$$

Here $A_1 = V_x^{(1)}(s)X'(s) + V_y^{(1)}(s)Y'(s)$, $A_2 = V_x^{(1)}(s)Y'(s) - V_y^{(1)}(s)X'(s)$, $\tilde{A}_1 = V_x^{(1)}(\frac{b}{2} - s)X'(\frac{b}{2} - s) + V_y^{(1)}(\frac{b}{2} - s)Y'(\frac{b}{2} - s)$ and $\tilde{A}_2 = V_x^{(1)}(\frac{b}{2} - s)Y'(\frac{b}{2} - s) - V_y^{(1)}(\frac{b}{2} - s)X'(\frac{b}{2} - s)$.

Next we map the fluid in the region 2 within a wavelength $-\lambda/2 < x < \lambda/2$ from the z-plane into the interior of the unit circle by the transformation

$$\zeta = e^{\frac{2i\pi z}{\lambda}}. \qquad (3.15)$$

https://doi.org/10.1017/S0956792504005790 Published online by Cambridge University Press

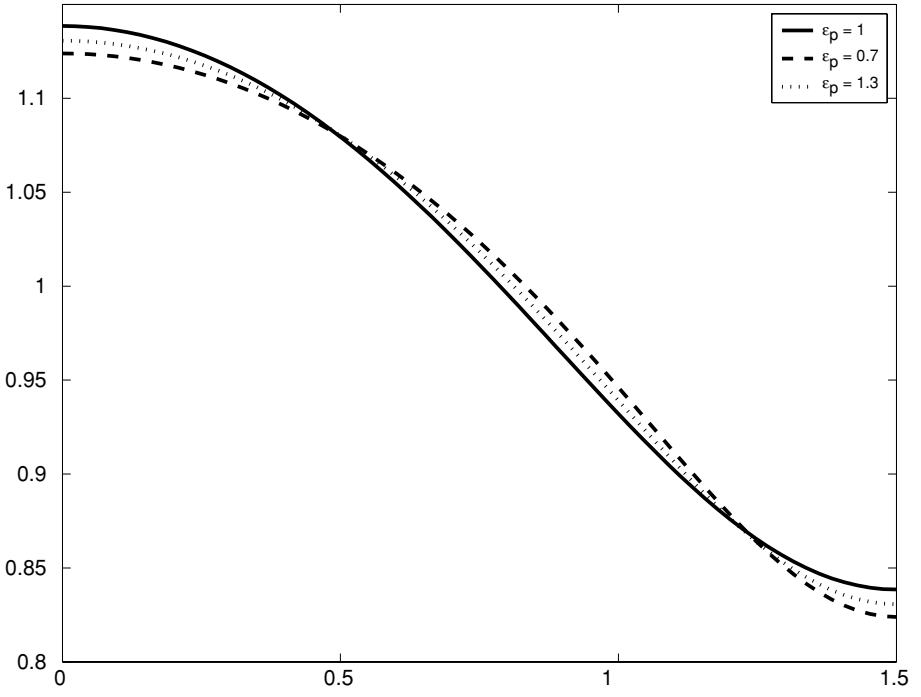


FIGURE 3. Antisymmetric traveling waves for different values of the permittivity; $\lambda = 3$, $E_b = 3$, $h = 0.3$. Solid curve $\epsilon_p = 1$; dotted $\epsilon_p = 1.3$; dashed $\epsilon_p = 0.7$.

Applying the Cauchy integral formula to the function $V_x^{(2)} - iV_y^{(2)}$ in the ζ-plane we obtain

$$V_x^{(2)}(t) = \frac{2}{\lambda}\mathrm{Im}\int_0^{\frac{b}{2}} \frac{[V_x^{(2)}(s) - iV_y^{(2)}(s)][iX'(s) - Y'(s)]}{1 - \exp\left(\frac{2i\pi}{\lambda}(X(t) - X(s)) - \frac{2\pi}{\lambda}(Y(t) - Y(s))\right)} ds$$
$$+ \frac{2}{\lambda}\mathrm{Im}\int_0^{\frac{b}{2}} \frac{[V_x^{(2)}(s) + iV_y^{(2)}(s)][iX'(s) + Y'(s)]}{1 - \exp(\frac{2i\pi}{\lambda}(X(t) + X(s)) - \frac{2\pi}{\lambda}(Y(t) - Y(s)))} ds, \tag{3.16}$$

where Im denotes the imaginary part.

We now use (2.18) and (2.19) and the relation $S_x = \frac{Y'(s)}{X'(s)}$ to express $V_x^{(1)}$ and $V_y^{(1)}$ in terms of $V_x^{(2)}$ and $V_y^{(2)}$ as

$$V_x^{(1)} = \frac{1}{1 + (Y'/X')^2}\left[V_y^{(2)}\frac{Y'}{X'}\left(1 - \frac{1}{\epsilon_p}\right) + V_x^{(2)}\left(1 + \frac{Y'^2}{X'^2\epsilon_p}\right)\right], \tag{3.17}$$

$$V_y^{(1)} = \frac{1}{1 + (Y'/X')^2}\left[V_y^{(2)}\left(\frac{Y'^2}{X'^2} + \frac{1}{\epsilon_p}\right) + V_x^{(2)}\frac{Y'}{X'}\left(1 - \frac{1}{\epsilon_p}\right)\right]. \tag{3.18}$$

Finally the kinematic boundary condition on the interface gives

$$uY'(s) - vX'(s) = 0. \tag{3.19}$$

https://doi.org/10.1017/S0956792504005790 Published online by Cambridge University Press

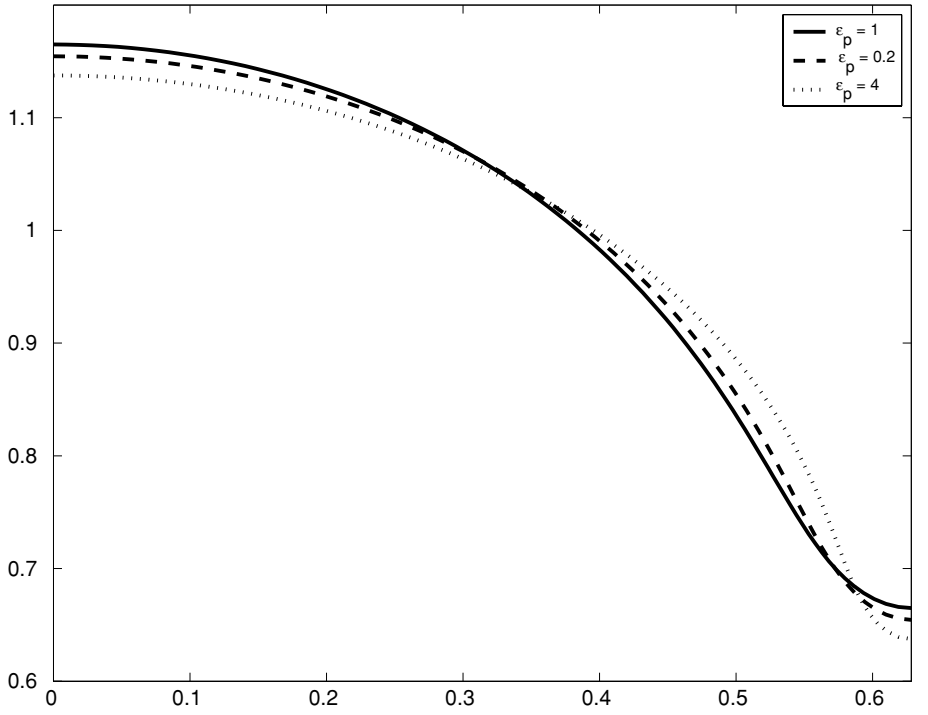


FIGURE 4. Symmetric traveling waves for different values of the permittivity; $\lambda = 2\pi/5$, $E_b = 155$, $h = 0.5$. Solid curve $\epsilon_p = 1$; dotted $\epsilon_p = 4$; dashed $\epsilon_p = 0.2$.

There are different ways to define the amplitude h. One way is to define it as the height between crests and troughs, i.e.

$$h = Y(0) - Y\left(\frac{b}{2}\right). \tag{3.20}$$

Another way is to define it as the L_2 norm of $Y - \delta$, i.e.

$$h = \left[\int_0^b [Y(s) - \delta]^2 X'(s) ds\right]^{\frac{1}{2}}. \tag{3.21}$$

The first one is used in the description of the results.

This completes the reformulation of the problem as a system of integro-differential equations. We seek six functions $X'(s)$, $Y'(s)$, u, v, $V_x^{(2)}$, $V_y^{(2)}$ and 3 parameters α, B and b satisfying (3.2), (3.3), (3.4), (3.13), (3.14), (3.16), (3.17), (3.18) (3.19), (3.20) (or (3.21)). These equations are solved numerically in the following Section.

4 Numerical method

In this section we outline the numerical method used to solve the system of integro–differential equations derived in the § 3.

https://doi.org/10.1017/S0956792504005790 Published online by Cambridge University Press

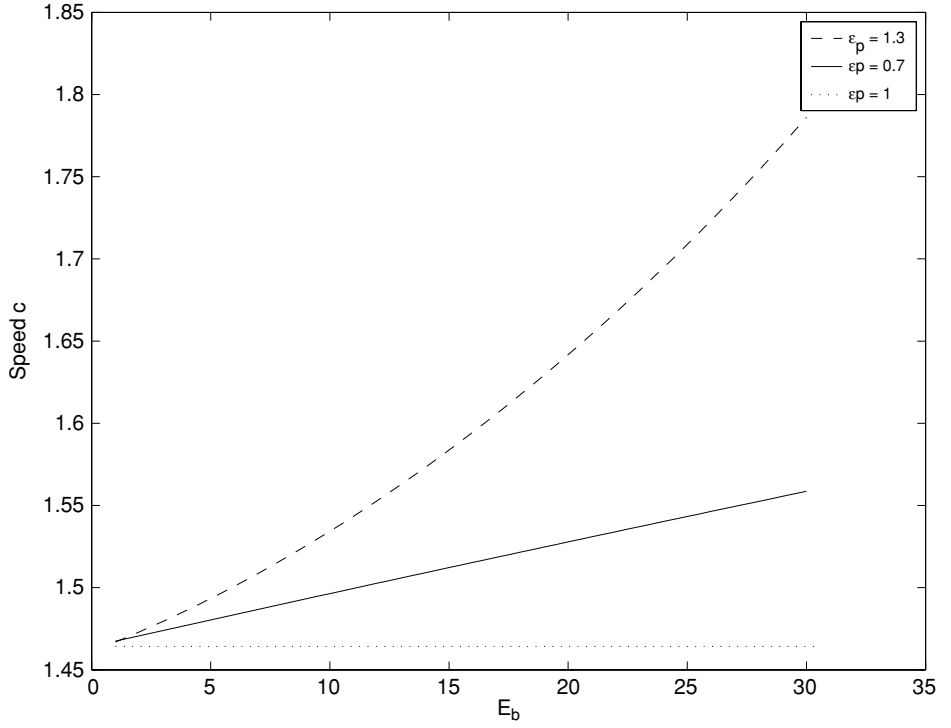


FIGURE 5. Variation of the wave speed c with applied electric field E_b. Results for $\lambda = 3$, $h = 0.3$, $\epsilon_p = 0.7$ (dashed), $\epsilon_p = 1.0$ (dotted) and $\epsilon_p = 1.3$ (solid).

We define equally spaced mesh points over the interval $[0, \frac{b}{2}]$ by the formulae

$$s_I = \frac{b}{2(N-1)}(I-1), \quad I = 1, \ldots, N \tag{4.1}$$

$$s_{I+\frac{1}{2}} = \frac{(s_{I+1} + s_I)}{2}, \quad I = 1, \ldots, N-1 \tag{4.2}$$

We also introduce the $6N$ unknowns $X'_I = X'(s_I)$, $Y'_I = Y'(s_I)$, $u_I = u(s_I)$, $v_I = v(s_I)$, $V_x^I = V_x^{(2)}(s_I)$ and $V_y^I = V_y^{(2)}(s_I)$.

We satisfy (3.1), (3.4) and (3.19) at the mesh points (4.1). This leads to $3N$ equations. $2N-4$ equations are obtained by satisfying (3.13) at the mesh points (4.2) , $I = 1, \ldots, N-2$ and (3.14) at the mesh points (4.2) , $I = 2, \ldots, N-1$. The integrals in (3.13) and (3.14) are approximated by the trapezoidal rule with a summation over the mesh points (4.1). The symmetry of the quadrature and of the discretisation enable us to evaluate the Cauchy principal vales as if they were ordinary integrals. Similarly we satisfy (3.14) at the mesh points (4.1), $I = 1, \ldots, N-2$ with a summation over the mesh points (4.2). Seven more equations are obtained by setting $v_1 = v_N = V_y^1 = V_y^N = 0$, $X(N) = 0.5\lambda$ and by imposing (3.10) and (3.7). One more equation is given by (3.20) or (3.21) with h prescribed.

The last equation expresses V_y^N in terms of V_y^I, $I = N-4, \ldots, N-1$ by a four point extrapolation formula. This gives a system of $6N + 3$ nonlinear algebraic equations for

https://doi.org/10.1017/S0956792504005790 Published online by Cambridge University Press

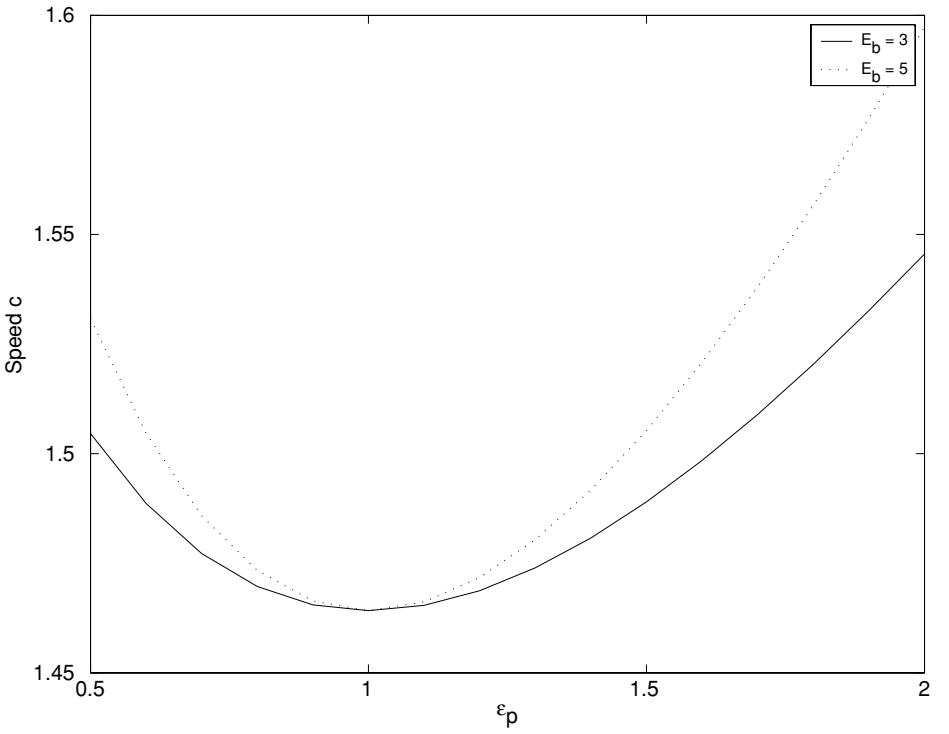


FIGURE 6. Variation of the wave speed c with the relative permittivity ϵ_p; results for fixed $\lambda = 3$, $h = 0.3$ and $E_b = 3$ (solid), $E_b = 5$ (dotted).

the $6N + 3$ unknowns B, c, α and $X_I', Y_I', u_I, v_I, V_x^I, V_y^I$, $I = 1, \ldots, N$. This system is solved by Newton's method.

5 Discussion of the results

We computed solutions for various values of λ, h, ϵ_p and E_b by using the numerical scheme of §4. The results presented were obtained with $N = 200$. We repeated the calculations with larger and smaller values of N and checked that all the results presented are independent of N within graphical accuracy.

A typical wave for $\lambda = 3$, $E_b = 3$, $h = 0.5$ and $\epsilon_p = 0.5$ is presented in Figure 2. We have shown several wavelengths of the wave. The profiles are nonlinear with broad crests (sharp crests) and sharp troughs (broad troughs) on the upper (lower) free surface.

When $\epsilon_p = 1$, the last term on the left hand side of (2.17) vanishes and the flow reduces to the capillary waves without electric fields of Kinnersey [11]. A profile for $h = 0.3$, $E_b = 3$ and $\lambda = 3$, obtained by using our numerical scheme, is shown in Figure 3 (solid curve). Here only one half of a wavelength of the top free surface is shown. The complete free surface profiles can be obtained by using (2.3). The profile is again nonlinear with a sharp trough and a rounded crest. As the amplitude is further increased the profile approaches a limiting configuration with a trapped bubble at its through (not shown here). The other profiles in Figure 3 show the influence of the relative permittivity of the fluid on waves produced for a fixed applied electric field. Here $E_b = 3$ and $h = 0.3$.

https://doi.org/10.1017/S0956792504005790 Published online by Cambridge University Press

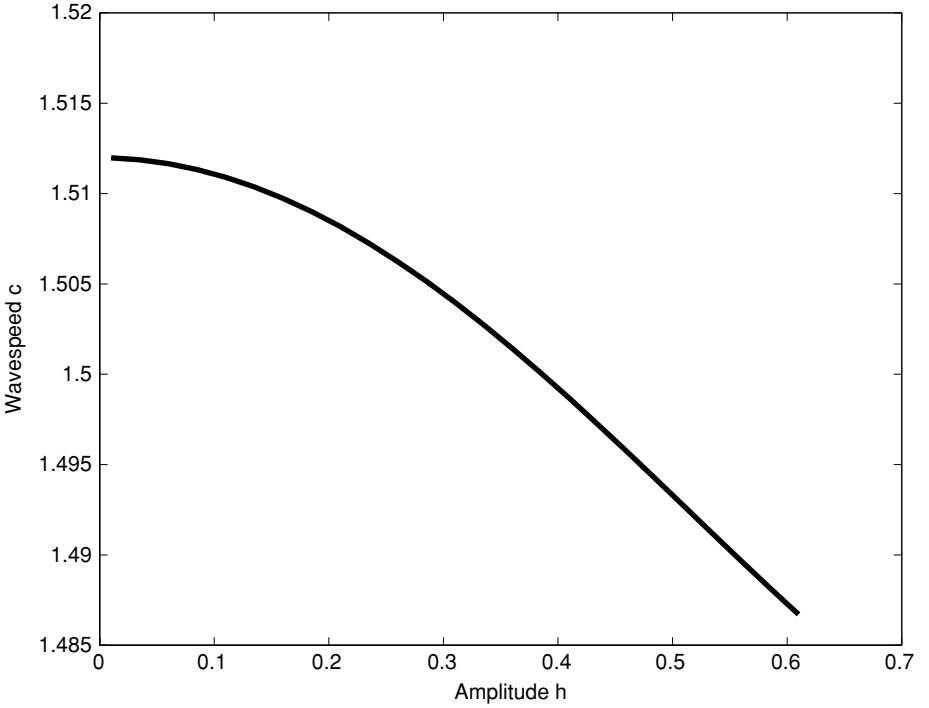


FIGURE 7. Variation of the wave speed with wave amplitude h; here $\epsilon_p = 0.5$, $\lambda = 3$ and $E_b = 3$.

As ϵ_p deviates from 1 the profiles become steeper. This trend appears to produce waves similar to the Kinnersley ones which approach trapped bubbles; the question of trapped bubble formation, however, remains open since we have not computed these due to the complications of having to solve the Laplace equation for the voltage potential in region 2. The same steepening property is found for the symmetric waves calculated by Papageorgiou & Vanden-Broeck [14]; we include sample results in this case in Figure 4. This Figure is included here for comparison and to update some of the results of Figure 2 of [14] which were computed for wrong values of the parameters.

In Figure 5, we present computed values of c versus E_b for $\lambda = 3$, $\epsilon_p = 0.7$, $\epsilon_p = 1$ and $\epsilon_p = 1.3$. The value of the amplitude of the traveling waves is taken to be $h = 0.3$. When $\epsilon_p = 1$, there are no electrical effects and the values of c do not depend on E_b. For $\epsilon_p < 1$ or $\epsilon_p > 1$, the curves are above of the horizontal line $\epsilon_p = 1$. This suggests that for given values of E_b and h, the velocity c of the wave is not a monotonic function of ϵ_p. This is confirmed in Figure 6, where we show values of c as a function of ϵ_p for $h = 0.3$, $E_b = 3$ and $E_b = 5$. This behavior can also be seen from the linear dispersion relation for a fixed wavelength. Note that this also holds for the symmetric waves studied in Papageorgiou & Vanden-Broeck [14].

Finally, we show in Figure 7 values of c versus h for $\epsilon_p = 0.5$, $\lambda = 3$ and $E_b = 3$. As can be expected for nonlinear dispersive waves, c is a function of h. As $h \to 0$ the values of c approach the linear value (2.29) predicted by writing $\omega = kc$ in (2.29) and solving for c.

https://doi.org/10.1017/S0956792504005790 Published online by Cambridge University Press

6 Conclusions

In this article, we have studied nonlinear antisymmetric interfacial waves of arbitrary amplitude and wavelength on electrified liquid layers. The electric field acts in a direction parallel to the undisturbed layer and we have included the effects of surface tension. Traveling waves have been computed using boundary integral techniques.

Our results show that the electric field has a significant effect on the shapes and speeds of nonlinear traveling waves. When the relative permittivity ϵ_p is different from unity, the waves become steeper relative to the non-electrifed case. The wave speed also increases when an electric field is present (see Figures 5 and 6).

We have also studied the variation of the wave speed as a function of the relative permittivity at different values of E_b (experimentally E_b can be increased by increasing the applied voltage drop). As can be seen in Figure 6, the wave speed increases when an electric field is applied irrespective of the value of ϵ_p. Larger values of E_b yield larger speeds. This non-monotonic behaviour as ϵ_p crosses the unit value, as well as the increase of the speed with E_b, can be clearly seen from the linear dispersion relation (2.29) where the electric field contribution is proportional to $E_b(1-\epsilon_p)^2$. Our results show that this trend holds into the nonlinear regime also.

The variation of the wave speed with wave amplitude has also been studied (see Figure 7). We find that the speed is a monotonic decreasing function of the wave amplitude with an upper bound provided by linear theory as the wave amplitude tends to zero.

In experiments, the scenario predicted for $\epsilon_p > 1$ is probably the most appropriate for our problem. Values of dielectric constants have been given in the microgravity liquid bridge experiments of Burcham & Saville [3]. The surrounding phase is a gas (sulphur hexafluoride) and the fluid is a certain oil (see Table 1 of Burcham & Saville). In all those systems, the value of ϵ_p ranges from 2.74 for the highest viscosity fluid (a silicon oil 12 M) to 5.24 for the lowest viscosity fluid (castor oil/Eugenol). Two-phase liquid-liquid systems were also used that have values of $\epsilon_p < 1$ (for example Silicon Oil 1 M surrounded by a less viscous Castor Oil/Eugenol – see Table 1 of Burcham & Saville [3]) which gives $\epsilon_p = 0.53$. Our theory needs to be modified in this case, however, to take into account the fluid dynamics of the surrounding phase. This is the subject of future research.

Acknowledgements

The work of DTP and JMVDB were supported by the National Science Foundation Grant number DMS-0072228 and DMS-0204808. The work was also supported by EPSRC and NATO.

References

[1] Blyth, M. G. & Vanden-Broeck, J.-M. (2004) New solutions for capillary waves on fluid sheets. *J. Fluid Mech.* **507**, 255–264.

[2] Blyth, M. G. & Vanden-Broeck, J.-M. (2004) New solutions for capillary waves on curved sheets of fluids. *IMA J. Appl. Maths*, accepted.

https://doi.org/10.1017/S0956792504005790 Published online by Cambridge University Press

[3] Burcham, C. L. & Saville, D. A. (2000) The electrohydrodynamic stability of a liquid bridge: Microgravity experiments on a bridge suspended in a dielectric gas. *J. Fluid Mech.* **405**, 37–56.

[4] Chen, B. & Saffman, P. G. (1979) Steady gravity–capillary waves on deep water. *Stud. Appl. Math.* **60**, 183–210.

[5] Crapper, G. D. (1957) An exact solution for progressive capillary waves of arbitrary amplitude. *J. Fluid Mech.* **2**, 532–540.

[6] Crowdy, D. G. (1999) Exact solutions for steady capillary waves on a fluid annulus. *J. Nonlinear Sci.* **9(6)**, 615–640.

[7] Hogan, S. J. (1980) Some effects of surface tension on steep water waves. Part 2. *J. Fluid Mech.* **96**, 417–445.

[8] Hunter, J. K. & Vanden-Broeck, J.-M. (1983) Solitary and periodic gravity-capillary waves of finite amplitude. *J. Fluid Mech.* **134**, 205–219.

[9] Jackson, J. D. (1963) *Classical Electrodynamics.* Wiley.

[10] Kang, Y. & Vanden-Broeck, J.-M. (2000) Gravity-capillary waves in the presence of constant vorticity. *Eur. J. Mech. B-Fluids*, **19**, 253–268.

[11] Kinnersley, W. (1976) Exact large amplitude capillary waves on sheets of fluid. *J. Fluid Mech.* **77**, 229–241.

[12] Maldarelli, C., Jain, R. K., Ivanov, I. B. & Ruckenstein, E. (1980) Stability of symmetric and unsymmetric thin liquid films to short and long wavelength perturbations. *J. Colloid Interface Sci.* **78**, 118.

[13] Melcher, J. R. & Schwarz, W. J. Jr. (1968) Interfacial relaxation overstability in a tangential electric field. *Phys. Fluids*, **11**, 2604–2616.

[14] Papageorgiou, D. T. & Vanden-Broeck, J.-M. (2004) Large amplitude capillary waves in electrified fluid sheets. *J. Fluid Mech.* **508**, 71–88.

[15] Ruckenstein, E. & Jain, R. (1974) Spontaneous rupture of thin liquid films. *J. Chem. Soc. Far. Trans. II*, **70**, 132.

[16] Savettaseranee, K., Papageorgiou, D. T., Petropoulos, P. G. & Tilley, B. S. (2003) The effect of electric fields on the rupture of thin viscous films by van der Waals forces. *Phys. Fluids*, **15**, 641–652.

[17] Scheludko, A. (1967) Thin liquid films. *Adv. Colloid Interface Sci.* **1**, 391.

[18] Schwartz, L. W. & Vanden-Broeck, J.-M. (1979) Numerical solution of the exact equations for capillary–gravity waves. *J. Fluid Mech.* **95**, 119–139.

[19] Taylor, G. I. (1959) The dynamics of thin sheets of fluid. II. Waves on fluid sheets. *Proc. Roy. Soc. Ser. A*, **253**, 296–312.

[20] Tilley, B. S., Petropoulos, P. G. & Papageorgiou, D. T. (2001) Dynamics and rupture of planar electrified liquid sheets. *Phys. Fluids*, **13**, 3547–3563.

[21] Vanden-Broeck, J.-M., Miloh, T. & Spivack, B. (1998) Axisymmetric capillary waves. *Wave Motion*, **27**, 245–256.

https://doi.org/10.1017/S0956792504005790 Published online by Cambridge University Press